Article

Using Spatial Structure Analysis of Hyperspectral Imaging Data and Fourier Transformed Infrared Analysis to Determine Bioactivity of Surface Pesticide Treatment

Christian Nansen [1,2,]*, Noureddine Abidi [3], Amelia Jorge Sidumo [2] and Ali Hosseini Gharalari [1]

[1] Texas AgriLife Research, 1102 East FM 1294, Lubbock, TX 79403 USA;
   E-Mail: AHosseini@ag.tamu.edu
[2] Department of Plant and Soil Science, Texas Tech University, Campus Box 42122, Lubbock, TX 79409 USA; E-Mail: asidumo@uem.mz
[3] Fiber and Biopolymer Research Institute, Department of Plant and Soil Science, Texas Tech University, Campus Box 45019, Lubbock, TX 79409 USA; E-Mail: N.ABIDI@ttu.edu

* Author to whom correspondence should be addressed; E-Mail: cnansen@ag.tamu.edu;
   Tel.: +1-806-746-6101; Fax: +1-806-746-6528.

Abstract: Many food products are subjected to quality control analyses for detection of surface residue/contaminants, and there is a trend of requiring more and more documentation and reporting by farmers regarding their use of pesticides. Recent outbreaks of food borne illnesses have been a major contributor to this trend. With a growing need for food safety measures and "smart applications" of insecticides, it is important to develop methods for rapid and accurate assessments of surface residues on food and feed items. As a model system, we investigated detection of a miticide applied to maize leaves and its miticidal bioactivity over time, and we compared two types of reflectance data: fourier transformed infrared (FTIR) data and hyperspectral imaging (HI) data. The miticide (bifenazate) was applied at a commercial field rate to maize leaves in the field, with or without application of a surfactant, and with or without application of a simulated "rain event". In addition, we collected FTIR and HI from untreated control leaves (total of five treatments). Maize leaf data were collected at seven time intervals from 0 to 48 hours after application. FTIR data were analyzed using conventional analysis of variance of miticide-specific vibration peaks. Two unique FTIR vibration peaks were associated with miticide application ($1,700$ cm^{-1} and 763 cm^{-1}). The integrated intensities of these two

peaks, miticide application, surfactant, rain event, time between miticide application, and rain event were used as explanatory variables in a linear multi-regression fit to spider mite mortality. The same linear multi-regression approach was applied to variogram parameters derived from HI data in five selected spectral bands (664, 683, 706, 740, and 747 nm). For each spectral band, we conducted a spatial structure analysis, and the three standard variogram parameters ("sill", "range", and "nugget") were examined as possible "indicators" of miticide bioactivity. We demonstrated that both FTIR peaks and standard variogram parameters could be used to accurately predict spider mite mortality, but linear multi-regression fits based on standard variogram parameters had the highest accuracy and were successfully validated with independent data. Based on experimental manipulation of HI data, the use of spatial structure analysis in classification of HI data was discussed.

1. Introduction

Many food products are subjected to quality control analyses before sold to consumers, and there is a trend of requiring more and more documentation and reporting by farmers regarding their use of pesticides. At the same time, reflectance-based quality control systems are becoming increasingly more versatile, robust and more affordable. Pesticide and contaminant (*i.e.*, fecal) residues and surface defects on vegetables and fruits [1-4] and meat [5] are of particular interest due to recent concerns about outbreaks of food borne illnesses [3]. Thus, among farmers, crop consultants, extension services, food processors, food distributors, and agricultural inspection entities there is a need for real-time tools to detect and quantify pesticides and other surface residues on food and feed materials. Precision agriculture [6,7], food quality and safety [8-11], and pharmaceutical industries [12] are just some of the areas in which reflectance-based analysis is becoming increasingly important. It is obviously important to continue improving the quality and robustness of spectral sensors, but it is equally important to develop classification algorithms that allow accurate, rapid and reliable processing and analysis of large reflectance data sets. Objects reflect electromagnetic energy according to their chemical composition, particle size, physical structure, and temperature [13], and different chemical bonds absorb and transmit light in uniquely different ways. The acquired signal of reflected electromagnetic energy is determined by the illumination source, projection angle, and type of spectral sensor. Reflection from a theoretically constant light source constitutes a "radiometric fingerprint", which are compared with reflectance data from training data set and subsequently classified/distinguished based on their chemical or physical properties. The driving factors behind widespread implementation of reflectance-based systems are: (1) data is acquired, processed and analyzed real-time due to increasingly faster and more powerful telecommunication systems and computer processing, (2) data acquisition is non-destructive, (3) labor intensive chemical procedures and/or qualitative/subjective evaluation procedures can be automated and replaced by quantitative standards, and (4) the technology is becoming increasingly cost-effective.

Fourier Transform Infrared spectroscopy (FTIR) is a rapid, non-destructive technique that can quantitatively detect a range of functional groups in the sample. It has been successfully used to investigate contaminated cotton fibers and yarn defects [14,15]. Furthermore, FTIR has emerged as a key technique for the study of plant growth and development [16-25]. Hyperspectral imaging (HI) data are acquired with line-scanning devices in which individual pixels are associated with a reflectance profile with reflectance values in narrow wavelength bands. Most HI sensors collect reflectance or transmission data within 350–2,500 nm (visible and near-infrared spectra).

Standard analytical approaches used in analysis of reflectance data include (see [9] for review): discriminant analysis [10,11,26], principal component analysis [3,21,26-28], multi-regression approaches, like partial least square (PLS) [12,29,30], use of spectral band ratios (indices) [3,31-33], decision trees [34], artificial neural networks [17,28,34], and support vector machines [8,35]. One common denominator in all of these analytical approaches is that they do not incorporate—or take advantage of —the spatial information available in a HI data.

Figure 1. Variogram illustrates relationship of distance between paired observations (lag distance) and variance, and variogram analysis is used to determine three parameters ("Nugget", "Range", and "Sill").
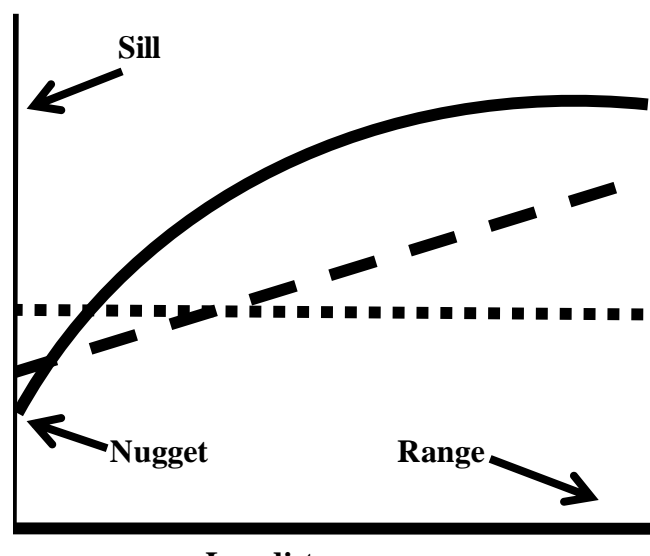
Spatial structure analysis can be conducted with reflectance data from HI cubes, because each pixel (hyperspectral profile) is associated with a set of x- and y-coordinates. Basically, the spatial structure of a data set describes how individual observations at individual points (in this case relative reflectance values in a single spectral band at a particular location within an image cube) are associated with their geographic position within the sampling universe. This geostatistical approach to imaging analyses is based on variogram analysis [36-39] which describes the distance between paired observations and the variance of observations of these paired observations (Figure 1). The spatial structure of a data set is either random or non-random. Random, or lack of spatial dependence, means that the variance of data is independent of the geographical distance between paired trap locations. Consequently, the curve fit is a straight line denoted "pure nugget variogram" [37] (dotted line in Figure 1). A data set with non-random spatial structure, shows spatial dependence [37,40] or spatial continuity [36], which

means that data points close to each other are generally more similar than observations at locations further apart. Spatial dependence is linear (dashed line in Figure 1) when the variance in counts increases proportionally with lag distance, or asymptotic when the variance of counts levels off after a certain lag distance and becomes constant (solid line in Figure 1). Asymptotic spatial dependence is the most commonly observed phenomenon, because it suggests that data points are spatially correlated up to a certain distance and then become uncorrelated. Once the variogram has been generated, a regression curve fit is used to characterize the spatial structure, and this regression fit includes three standard parameters, "nugget", "range", and "sill". The nugget represents an estimate of the variance between observations collected at "zero distance apart", which equals the noise or stochasticity in the data set. The range is an estimate of the maximum distance at which point observations are spatially auto-correlated, beyond this distance point observations are to be considered spatially uncorrelated. As the distance between point observations increase, the variance asymptotically approaches the sill, which is an estimate of the total variance explained within the spatial structure analysis. For instance, in ecology, it is often seen that environmental observations collected in close proximity to each other are more similar than observations collected further apart. Thus, variance among paired observations is correlated to the distance between points. Analysis of the spatial structure of reflectance values in a single spectral band can be used as indicator of plant stress [41]. The underlying assumption in these studies is that reflectance data from a healthy crop leaf are more uniform than those acquired from a stressed crop leaves. A change in variance among adjacent spectral profiles will inherently cause a change in standard variogram parameters. The exact biological meaning of these three standard variogram parameters is not fully understood, but the use of variogram parameters as indicators of crop stress was a more consistent analytical approach more conventional analyses of mean/variance reflectance values and standard indices.

In this study, we investigated the hypothesis that standard variogram parameters can be used to assess the bioactivity of a miticide applied to crop leaves. We applied a miticide [Acramite (Chemtura Corporation, Middlebury, CT. AI: bifenazate)] at a known rate to portions of maize leaves under field conditions and subsequently tested spider mite mortality and conducted Fourier transformed infrared analysis (FTIR) and HI analyses of treated and untreated maize leaves. We examined miticide applications with or without addition of a surfactant and with or without a subsequent simulated rain event. Variogram analysis was used to identify standard variogram parameters from each experimental unit, while FTIR data were analyzed using conventional parametric statistics. We examined to what extent absolute FTIR peak values acquired from maize leaves were associated with spider mite mortality. Standard variogram parameters from HI analysis acquired from maize leaves were also examined as possible explanatory variables of spider mite mortality. A training regression model of HI data was successfully validated with an independent data set. As part of a "robustness test", HI data were experimentally manipulated (systematic and random changes in reflectance values), and we evaluated the effects of data manipulations on variogram parameters. Based on experimental re-manipulation of HI data, we discuss the use of spatial structure analysis in classification of HI data.

2. Materials and Methods

2.1. Experimental Design

2.1.1. Treatment with Miticide of Maize Leaves Under Field Conditions

Data were collected from a maize field plot (50 m wide and 50 m long) at the Texas AgriLife Research and Extension Center in Lubbock, TX, USA. The maize was planted on June 2 and leaf data were collected at tasseling stage on two separate dates (data set 1: July 30, 2008, data set 2: August 6, 2008). Within each of 5 rows, we selected 32 plants, 3–5 plants apart, and all selected plants within each row were treated the same way (see below). The 10 cm diameter mid portion of the 7th or 8th leaf (counting from the lowest leaf) on a maize plant constituted the experimental unit in this study, and only one leaf on each selected plant was included. Data set 1 included five treatments including miticide (Chemtura Corporation, Middlebury, CT. AI: bifenazate) at a single rate [4.7 nL/cm^2 (12 ounces per acre) in a 1.5 μL/cm^2 (20 gallon per acre) water formulation]: (1) miticide only and no rain event, (2) miticide only and rain event, (3) miticide and a surfactant but no rain event, (4) miticide and a surfactant and rain event, and (5) no treatment (untreated control). The used application rate of the surfactant, Silwet L-77 (Setre Chemical Company, Memphis, TN, USA), was 1.0 nL/cm^2 (2.5 ounces per acre). Data set 2 included 10 treatments: miticide (bifenazate) applied at four rates [4.7 (12 ounces per acre), 6.3 (16 ounces per acre), 7.8 (20 ounces per acre), and 9.4 (24 ounces per acre) nL/cm^2 in a 1.5 μL/cm^2 (20 gallon per acre)] water formulation) with/without rain event, and we included untreated controls (negative control) and water only treatment (positive control).

The miticide was applied onto carefully marked (marked with a sharpie) portions of leaves in the field, using a custom-built device, here referred to as the "bottle sprayer" [41]. In brief, the bottle sprayer consists of an airbrush (Master Airbrush model G22, TCP Global®, San Diego, CA, USA) inside a plastic funnel which is inside a 2-liter soda bottle, spraying at a fixed distance (20 cm). A CO_2 gas cylinder with corresponding regulator (JO Series, Compressed Gas Regulator, Chudnow, MFG. CO. Inc., Oceanside, NY, USA) and connecting tubes provide a controlled and consistent pressure. Based on a priori calibration, we used a CO_2 pressure of 10 psi and sprayed for 1 second (measured with a metronome). In data set 1, all five treatments (including untreated control) were applied to each of 32 experimental units at two pm (total of 160 experimental units), and four replicated experimental units were collected at 0, 1, 4, 6, 12, 24, and 48 h later. In data set 2, all treatments were applied at two pm and collected two hours later. Regarding treatments involving simulated rain, we used a transformed 2-liter soda bottle with a perforated bottom, and it was held 20 cm above the leaf when simulating the rain event. Perforations were made in a regular grid (1 cm between holes) with a total of 52 perforations. Preliminary analysis of the last five years weather data obtained from weather stations located on the Southern High Plains indicated that most rain events produce 2.5–12.5 mm water. Therefore, the equivalent of 13 mm rain fall was applied to experimental units as a simulated rain event. Ideally, leaf samples should be collected from maize plants, which had been sprayed according to commercial standards. However, dosage of miticide applied to individual leaves varies tremendously—both within and between plants (this can be tested easily by comparing water sensitive spray cards placed in fields prior to pesticide application). Although, used methods for applying both miticide and simulate rain provided applications that were different from 'real-world' applications,

they permitted us to acquire highly repeatable data. Immediately after collection of leaf material, experimental units were placed on dry ice and transferred to laboratory conditions and divided into three parts: ½ for spider mite bioassay, ¼ for FTIR analysis, and ¼ for HI analysis.

2.1.2. Spider Mite Bioactivity

In analyses of agro-chemicals applied to crops, there are multiple chemical-based techniques, including high pressure liquid chromatography, to quantify the amount applied. However, in studies of pesticides, the most valuable information is whether a given application is efficacious or not—whether it provides control of the target pest or not. Thus, in this study we did not quantify how much miticide was applied to each leaf but examined its "bioactivity" against spider mites (Tetranychidae). Spider mites are important pests on maize in the southern high plains [42]. Spider mites used in this study originated from naturally infested maize fields near Lubbock (TX, USA) in the summer of 2007, and they had been reared on maize plants in a greenhouse at the Texas AgriLife Research and Extension Center (Lubbock, TX, USA). The spider mite bioassay was conducted in Petri dishes (100×15 mm) containing a 2.3 % water agar solution. In each bioassay, maize leaf pieces (6×4 cm) were placed on water agar solution with the top side upwards. Three adult female mites were transferred to each maize leaf piece. Within five min after transfer to Petri dishes, spider mites were observed to ensure they were alive and behaved normally. In this spider mite bioassay, Petri dishes were kept under ambient conditions in a laboratory (19–21 °C and 40–60% RH), and spider mite survival and mortality were assessed 48 h after infestation.

2.2. Fourier Transformed Infrared Spectroscopy (FTIR)

FTIR spectra of maize leaves were recorded in an environmentally-controlled laboratory (21 ± 1 °C and 65 ± 2% RH) using the Spectrum-One equipped with an UATR (Universal Attenuated Total Reflectance) accessory (PerkinElmer, USA). The UATR-FTIR was equipped with a ZnSe-Diamond crystal composite that allows collection of FTIR spectra directly on a sample without any special preparation. The instrument is equipped with a "pressure arm" which is used to apply a constant pressure to maize leaves positioned on top of the ZnSe-Diamond crystal to ensure a good contact between the sample and the incident IR beam. The amount of pressure applied is monitored by the Perkin-Elmer FTIR software. We collected 30 FTIR spectra from each maize leaf. All FTIR spectra were collected at a spectrum resolution of 4 cm^{-1}, with 32 co-added scans over the range from 4,000 cm^{-1} to 650 cm^{-1}. A background scan of clean ZnSe-Diamond crystal was acquired before scanning the samples. The Perkin-Elmer software was used to perform spectra normalization, baseline corrections, and peak integration. Data set 1 was used for FTIR analysis. Comparisons of absorption spectra from miticide-treated and untreated maize leaves were used to identify the FTIR bands that were specific to the miticide. Spectra of pure miticide were also collected as a reference (standard). After baseline correction and normalization, the integrated peak intensities of specific peaks were determined.

2.3. Hyperspectral Imaging (HI)

We used a line-scanning hyperspectral camera (PIKA II, www.resonon.com) acquiring 160 spectral bands within the wavelength range from 405 to 907 nm (wavelength resolution of 3.1 nm) mounted on an aluminum tower-structure about 35 cm above a Petri dish (9-cm diameter) holding individual maize leaf pieces. Details about the image acquisition conditions are available in [11]. Hyperspectral images of individual maize leaf pieces were acquired at a magnification representing about 166 hyperspectral profiles (pixels) per mm^2. All hyperspectral images were collected in a dark room, and artificial lighting consisted of two 12V 20W 20° and four 12V 5W 30° halogen light bulbs mounted in two angled rows—one on either side of the lens. As lighting power source, we used a voltage stabilizer (Tripp-Lite®, PR-7b, www.radioreference.com). A piece of white Teflon (K-Mac Plastics, MI, USA) was used for calibration, and for each spectral band, hyperspectral reflectance profiles were converted into proportions of the reflection from Teflon (denoted relative reflectance). The hyperspectral camera used in this study has 640 sensors in linear array, and an image representing 100 lines/frames is equal to 64,000 hyperspectral profiles or pixels (3.85 cm^2), which was collected from each piece of maize leaf. Each image data file was imported into PC-SAS 9.1 (SAS Institute Inc., Cary, NC, USA) for statistical analysis. In data set 1 (training data), comprising of five treatments, seven time points, and four replications, we acquired spectral data from 140 experimental units. In data set 2 (validation), comprising of three treatments and four replications, we acquired spectral data from 12 experimental units.

2.4. Non-Spatial Statistical Analysis

The statistical analyses of both FTIR and HI data were based on examination of the following four treatment effects: miticide treatment (denoted "miticide") (yes = 1/no = 0), surfactant (yes = 1/no = 0) (denoted "surfactant"), rain event (yes = 1/no = 0) (denoted "rain"), and time between treatment and collection of leaf (0–48 hours) (denoted "time"). Finally, the response variable "bioactivity" refers to spider mite mortality from the bioassay (see above). All data were analyzed using procedures in PC-SAS 9.1 (SAS Institute Inc., Cary, NC, USA). Analysis of variance (PROC MIXED) was used to examine the four treatment effects on spider mite mortality in data set 1. Separate analyses were conducted for each time interval.

In the analysis of FTIR analysis of data set 1, only two peaks (1,700 cm^{-1} and 763 cm^{-1}) appeared to be consistently associated with miticide applications, and a linear regression analysis with forward stepwise selection option (PROC REG) was conducted with spider mite bioactivity as response variable and the following six explanatory variables: vibration peaks at 1,700 cm^{-1} and 763 cm^{-1}, "miticide", "surfactant", "rain", and "time". The forward selection of the six explanatory variables with significant contributions was based on calculation of F-statistics.

In the analysis of HI data, we compiled spectral data from time 0 (5 treatment classes × 4 replications × 64,000 hyperspectral profiles = 1,280,000 hyperspectral profiles) and conducted a stepwise discriminant analysis (PROC STEPDISC) based on calculation of F-statistics with bioactivity as response variable to determine which five spectral bands that provided the best indication of miticide treatment immediately after the miticide application had occurred (664, 683, 706, 740, and 747 nm). Separate analyses of variance (PROC MIXED) were conducted to examine effects of the

four treatment effects ("miticide", "surfactant", "rain", and "time") on average reflectance values in those five spectral bands.

2.5. Spatial Statistical Analysis

Spatial structure analysis of HI data was based on variogram analysis and the selection of spectral bands was based on an *a priori* stepwise dicriminant analysis. We conducted a total of 140 variogram analyses (PROC VARIOGRAM) of data from data set 1 and 12 from data set 2 for each of the five spectral bands (total of 760 variogram analysis, each based on 64,000 data points). In each variogram analysis, we used the following settings: lag distance = 1, maxlags = 10, outpdistance = 100. The variogram (relationship between distance between paired observations and variance) was fitted to a commonly used regression model [39]:

$$Equation \quad 1: \quad F(v) \quad = \quad a + b\left(1 - e^{\left(\frac{-3 \times D}{c}\right)}\right)$$

In which "a-c" are fitted coefficients. The main conveniences of using Equation 1 for model fit of the spatial structure are that "a" denotes the nugget, "b" the sill, and "c" the "range".

We conducted analyses of variance for each combination of spectral band and standard variogram parameter and examined their response to the four treatment effects. In addition, we conducted a linear multi-regression analysis (PROC REG) with forward selection option with bioactivity as response variable and the following explanatory variables: the four treatment effects ("miticide", "surfactant", "rain", and "time") and standard variogram parameters for each of the five selected spectral band (664, 683, 706, 740, and 747 nm). The forward selection of the six explanatory variables with significant contributions was based on calculation of F-statistics. A separate multi-regression analysis was conducted for each of the five spectral bands. The five linear regression fits were validated with an independent data set (data set 2), and the relationship between observed and predicted was examined.

We constructed an experimental HI data set from a single spectral band (683 nm) of an untreated maize leaf. This data set was chosen as a priori analysis showed that it was representative for HI data sets acquired from untreated maize leaves. The 64,000 reflectance values were sorted by descending x- and y-coordinates, and all reflectance values were multiplied by either 1.025 or 1.050 to simulate a 2.5% and 5.0% increase in all reflectance values. We also conducted random selections of reflectance values and multiplied half the values with 1.025 and one-third of the reflectance values with 1.050—to simulate random increase to simulate, for instance, spray application of a comparatively brighter material onto the leaf surface. The actual variogram parameters from the non-manipulated data were compared with variograms from the four manipulations.

3. Results

3.1. Spider Mite Bioassay

The spider mite bioassay enabled us, in a repeatable and controlled manner, to determine the bioactivity of the miticide. Of the four treatment effects, only miticide was significant (df = 1, 128, F-value = 160.9, P < 0.001), and although mortality in untreated controls was slightly higher than

expected, the miticide provided >80% mortality on most treated leaves (Figure 2). In the pairwise contrasts for each time interval between miticide application and rain event, we found a consistent significant effect of miticide treatment, while effects of rain event and/or addition of surfactant appeared to have negligible and/or inconsistent effects on the performance of the miticide (Table 1).

Figure 2. Average miticide bioactivity (spider mite mortality) from different treatments. Statistical analyses of spider mite bioassay results are presented in Table 1.
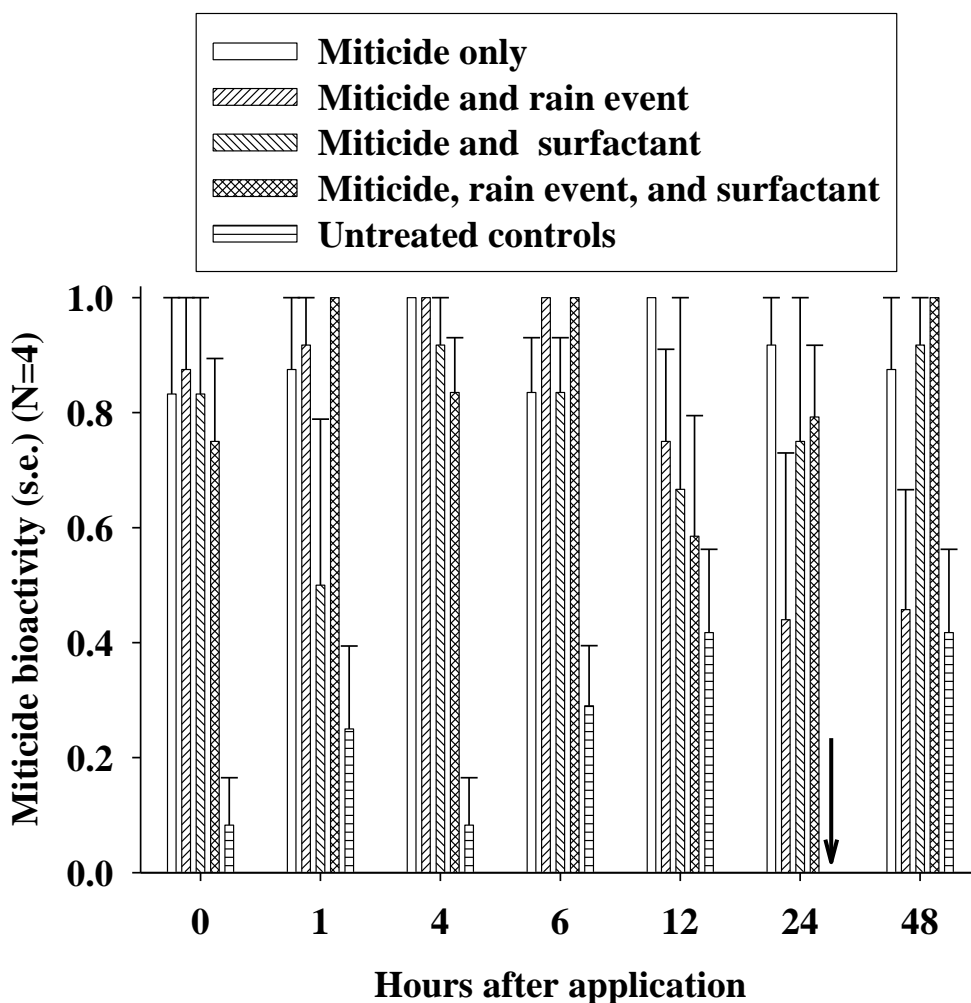

**Table 1.** F-values from pairwise comparisons of miticide treatments (analysis of variance).

Contrast	Effect	Hours after miticide application							
		0	1	4	6	8	12	24	48
1 *vs.* 5	Acramite no water	14.15**	7.71*	92.76***	25.52***	19.76***	5.41*	8.4*	6.02*
1 *vs.* 2	Acramite and water	0.05	0.04	0.01	2.34	5.99*	1.02	2.88	5.02*
3 *vs.* 4	Acramite/surfactant and water	0.17	4.94*	0.75	2.34	0.32	0.09	0.03	0.21
1 *vs.* 3	Surfactant no water	0.01	2.78	0.75	0.01	1.03	1.52	0.42	0.05
2 *vs.* 4	Surfactant and water	0.39	0.13	3.01	0.01	0.74	0.43	1.56	8.47*

Hours between miticide application and leaf collection "*": Contrast numbers refer to treatment classes, and separate analyses of variance were conducted for each time point. "*": significant difference with P < 0.05, "**": significant difference with P < 0.01, "***": significant difference with P < 0.001.

3.2. FTIR Analysis

Figure 3 shows the FTIR spectra of untreated maize leaf (green), maize leaf treated with miticides without rain event (blue), and maize leaf treated with miticides with rain event 1 h after miticide application (red). Specifically peaks located at 3,313 cm^{-1}, 1,700 cm^{-1}, and 763 cm^{-1} appeared to be associated with miticide application, and these peaks were also present in the spectrum of pure miticide (not shown). The vibration located at 3,313 cm^{-1} is attributed to N-H stretching, the vibration located at 1,700 cm^{-1} is attributed to C=O stretching, and the vibration located at 763 cm^{-1} is attributed to N-H out-of-plane bending [43]. Both vibrations at 1,700 cm^{-1} and 763 cm^{-1} were uniquely associated with miticide application and not found in FTIR spectra from untreated controls. The results showed highly significant effects of both miticide and surfactant on both vibration peaks ($P < 0.001$). Regarding the vibration peak at 1,700 cm^{-1}, we also obtained a significant effect of rain (df = 1,135, F-value = 3.92, P-value = 0.049), but there was no significant effect of time for any of the two vibration peaks ($P > 0.050$). In the linear multi-regression analysis of bioactivity, only two variables, miticide and vibrations at 1,700 cm^{-1}, contributed significantly to the regression fit (df = 2, 138, adjusted R^2-value = 0.490, F-value = 67.20, P-value < 0.001). The FTIR-based detection of bioactivity explained about 50% of the variance, which was considerably lower than was obtained based on spatial structure analysis of HI data (see below), so although significant and interesting because of unique miticide vibration peaks, the FTIR approach was not pursued further.

Figure 3. Fourier transformed infrared analysis (FTIR) spectra from maize leaves. Untreated control maize leaf (in green), maize leaf treated with miticide before rain event (blue), and maize leaf treated with miticide after simulated rain (red).
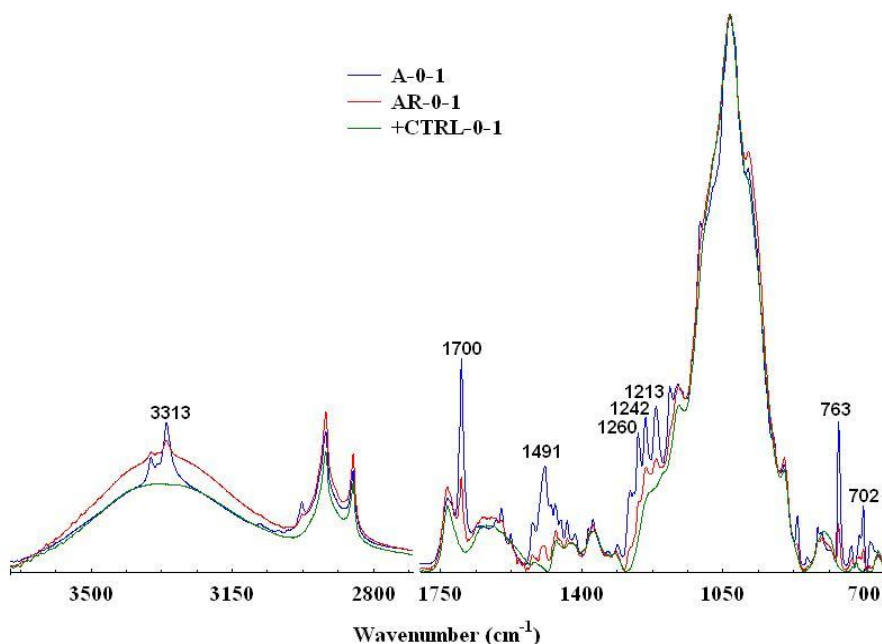
3.3. Regression Analysis of Average Hi Data per Leaf

Hyperspectral data were collected from small pieces of maize leaf (3.85 cm^2) (**a**). Average hyperspectral profiles from untreated maize leaves (**b**) and leaves treated with miticide (**c**) 0, 4, 12, and

48 hours after miticide application. Difference (untreated/treated) between the two treatments is also presented (**d**).

Figure 4. Average hyperspectral profiles acquired from untreated and miticide-treated maize leaves over time.
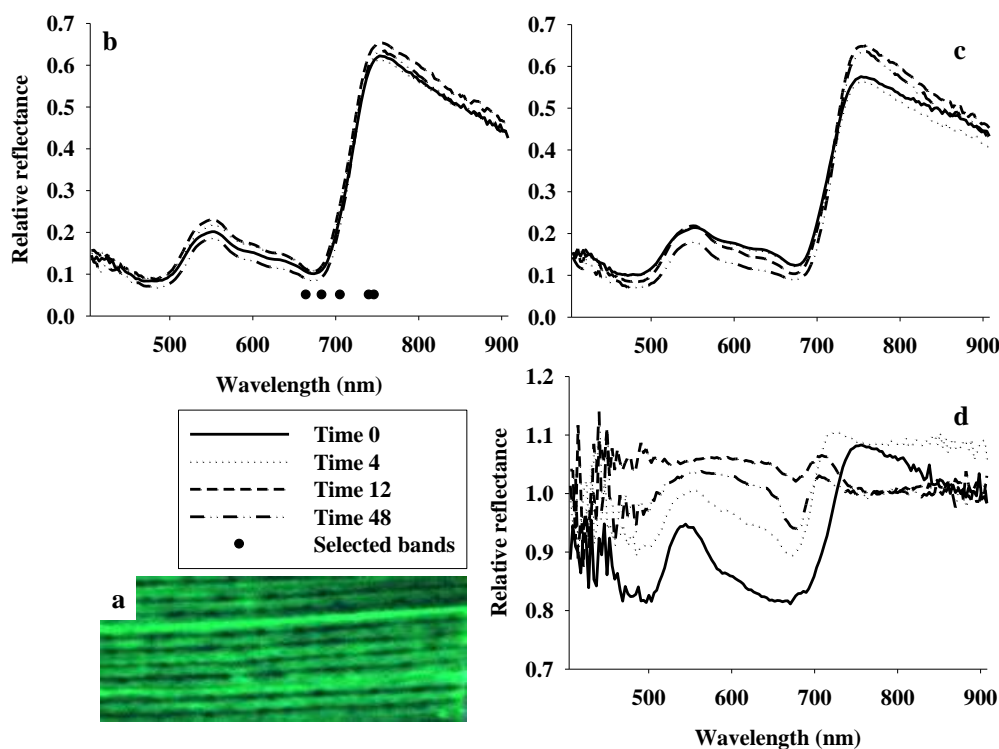

Figure 4 shows a representative RGB image of maize leaves after hyperspectral image acquisition (Figure 4a), and average hyperspectral profiles from two of the five treatments [untreated controls (Figure 4b) and maize leaves treated with miticide only (Figure 4c)]. It was seen that average profiles within treatments varied considerably, and it was also seen that the relative ratio over time between the two treatments was not constant (Figure 4d). Thus, it appeared that any analysis based on relative reflectance values would not be very accurate over time. In the initial stepwise discriminant analysis of 1,280,000 hyperspectral profiles, reflectance at the following wavelengths had the highest contributions to the separation of the five treatment classes: 664, 683, 706, 740, and 747 nm (Figure 4b), so only data in these spectral bands were analyzed. There was a significant time trend in all five spectral bands, but no significant effect of miticide on bioactivity but a significant effect of surfactant in two of the spectral bands (Table 2). We obtained a significant regression fit of bioactivity with average reflectance in the five spectral bands and the four treatment effects as explanatory variables (df = 3,134, adjusted R^2-value = 0.443, F = 36.46, P < 0.001), when based on three explanatory variables (miticide, surfactant, and reflectance at 747 nm). About 45% of the total variance was explained, which was considerably lower than was obtained based on spatial structure analysis of HI data (see below).

Table 2. F-values from analysis of variance of average reflectance data in five spectral bands.

Effect	Spectral band (nm)				
	664	706	740	683	747
Miticide	1.1	0.09	0.01	0.73	0.10
Surfactant	0.1	0.61	9.24**	0.18	10.00***
Water	1.32	0.46	1.42	0.83	1.14
Time	14.02***	8.51***	2.33*	11.3***	2.28*

Miticide treatment (yes/no), time between miticide application and leaf collection, surfactant (yes/no), rain event (yes/no) were used as explanatory variable of relative reflectance, and statistics from regression fits to both training and validation data sets are provided. "*": significant difference with $P < 0.05$, "**": significant difference with $P < 0.01$, "***": significant difference with $P < 0.001$.

3.4. Spatial Structure Analysis of HI Data

Based on 700 separate spatial structure analyses (140 for each of the five spectral bands), it was seen that nugget values and range values in all five spectral bands showed a highly significant time trend, while there was only sporadic significant effects by the other three treatments (Table 2). In other words, the standard variogram parameters did not appear to respond as clearly to treatment effects as FTIR vibration peaks. However, we used multi-linear regression with forward selection to determine to what extent the three standard variogram parameters and the four treatment effects could explain bioactivity. For all five spectral bands, we obtained significant curve fits and were able to explain >62% of the total variance (Table 3). Miticide treatment, surfactant, and the nugget parameter contributed significantly to all five regression analyses. Rain effect did not contribute significantly to any of the regression fits, while the range parameter and time effect only contributed significantly to the regression fit that involved standard variogram parameters of reflectance data at 747 nm.

Table 3. Parameters and coefficients from regression fits to miticide bioactivity based on variogram parameters (Nugget, Sill, and Range) and treatment factors (miticide, surfactant, and time).

Wavelength (nm)	Explanatory Variables						Training Adj R^2-value	Validation Adj R^2-value
	Nugget	Sill	Range	Miticide	Surfactant	Time		
664	702.11	88.66		0.059	−0.061		0.639	0.961
706	202.07	44.29		0.059	−0.038		0.629	0.961
740	69.1			0.059	−0.048		0.645	0.96
683	475.14	58.00		0.059	−0.057		0.641	0.962
747	56.44		0.002	0.059	−0.055	−0.003	0.649	0.958

Forward selection based on F-statistics were used to select variogram parameters and treatment effects that contributed significantly to regression fits to miticide bioactivity (Figure 2). Regression models were developed based on data set 1 and validated with data set 2.

3.5. HI Validation and Parameter Investigation

Spatial structure analysis was conducted based on data set 2, and the 12 sets (Three treatment classes and four replications) of standard variogram parameters were validated based on the coefficients in Table 3. All five validations (each of the five spectral bands) were highly significant with adjusted coefficients of determination (adjusted R^2-value) > 0.96 (Table 3). The correlation between observed and predicted bioactivity was highest using standard variogram parameters from the spectral band at 683 nm with predicted bioactivity as a function of a range of nugget and sill values (surfactant and miticide treatment were kept constant at 1 and 12, respectively). The coefficients in Table 3 suggest that even a fairly small increase in nugget value causes a marked increase in predicted bioactivity. A follow-up question is therefore: what change in a HI data set will change the spatial structure with particular reference to the nugget value? We addressed this question through experimental manipulation of reflectance data at 683 nm data from an untreated maize leaf. The following manipulations were examined: (1) increase all 64,000 reflectance values by 2.5% or 5.0%, or (2) randomly increase half or one-third of the reflectance values at 683 nm by 2.5% or 5.0%, respectively. Figure 5 shows that increasing all reflectance values by 2.5% caused an increase in nugget value by about 5% (from 0.0034 to 0.0036) and sill value by about 5% (0.00059 to 0.00062), and increasing all reflectance values by 5.0% caused an increase in nugget value by about 10% (from 0.0034 to 0.0079) and sill value by about 10% (from 0.00059 to 0.00065). On the other hand, range values were unaffected. Thus, the increase in stochastic variance (nugget value) and total variance explained by the spatial structure was twice the increase in reflectance values. Figure 4 also showed that randomly increasing portions of the reflectance values appeared to have comparatively highest impact on nugget values.

Figure 5. Variogram analysis of reflectance data from single spectral band (683 nm) of an untreated maize leaf were experimentally manipulated in four ways and compared with actual: multiplying all reflectance values with either 1.025 or 1.050 to simulate a 2.5% and 5.0% increase in all reflectance values or multiplying half the reflectance values (random selection) w   ith 1.050.
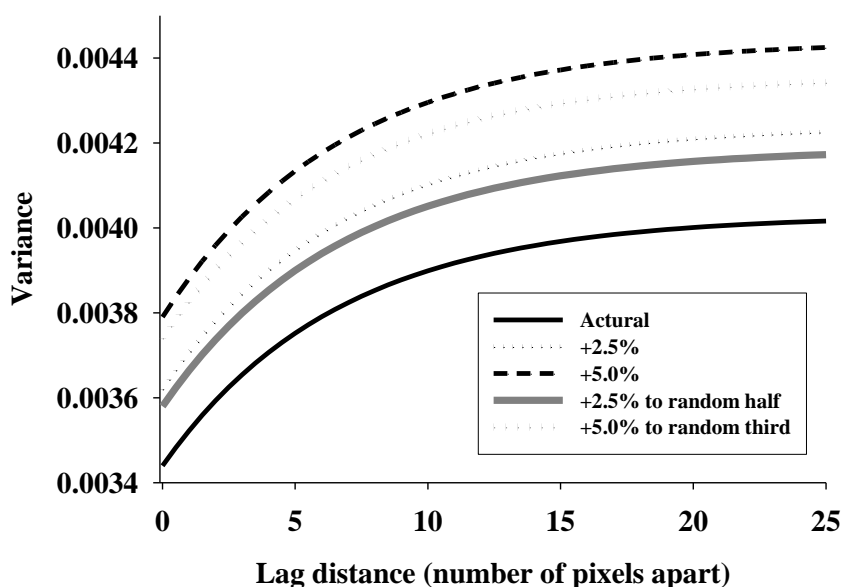
4. Discussion

Reflectance-based analyses are becoming increasingly important in agriculture and elsewhere, because the technology is highly sensitive and therefore can be used to classify/distinguish objects with only subtle physical or chemical differences. There are many chemical-based approaches to residue analysis of insecticides on crops and food items, such as, HPLC [44,45], ELISA [46], gas chromatography [47,48]. While all of these methods are highly accurate and able to detect very low residue levels, they require specially trained personnel, fairly sophisticated laboratory conditions, and are time-consuming. The two analytical approaches used in this study also require certain equipment capabilities but both are non-destructive procedures that require a minimum of sample preparation, and they both have the potential of providing results real-time. Due to high sensitivity of reflectance-based technologies, it is common to see prediction accuracies of training data sets exceeding 85%, but the real test is how well a given classification algorithm performs on independent data sets. Independent validations are not always included, and several authors have highlighted some of the challenges associated with radiometric noise/stochasticity in reflectance-based studies [49,50]. It was within this context that the potential of spatial structure analysis of HI data was investigated and compared with analysis of FTIR data.

This study showed that: Two unique FTIR vibration peaks were associated with miticide application (1,700 cm^{-1} and 763 cm^{-1}). The integrated intensities of these two peaks, miticide application, surfactant, rain event, time between miticide application, and rain event were used successfully as explanatory variables in a linear multi-regression fit to spider mite mortality. Reference [20] used FTIR to characterize isolated endodermal cell walls from plant roots and assigned FTIR frequencies to functional groups present in the cell wall, including the relative amounts of the cell wall biopolymers suberin and lignin, as well as cell wall carbohydrates and proteins. FTIR absorption spectra indicated structural differences for three developmental stages of the endodermal cell wall under study. The authors concluded that FTIR could be used as a direct and non-destructive method suitable for the rapid investigation of isolated plant cell walls. The approach has since been successfully applied to screen large numbers of mutants for a broad range of cell wall phenotypes using FTIR of leaves of *Arabidopsis thaliana* and flax (*Linum usitatissimum*) [21]. Also, FTIR and Fourier-Transform Raman spectroscopy have been successfully used to investigate the primary cell wall architecture at a molecular level [23] Dynamic changes in cell wall composition of hybrid maize coleoptiles (*Zea mays*) were investigated by FTIR [17].

Spatial structure analysis is a novel approach to analysis of ground based remote sensing data, but it can only be applied to data sets in which reflectance data are georeferenced (*i.e.*, associated with a pixel in an image cube). Published studies suggest that the spatial structure of reflectance data within a given spectral band may be more consistent over space and time (and therefore less susceptible to radiometric stochasticity) than absolute reflectance values [51]. The same linear multi-regression approach applied to FTIR vibration peaks was also applied to average reflectance peaks and variogram parameters (both derived from HI data in five selected spectral bands: 664, 683, 706, 740, and 747 nm). Highest accuracy was obtained using variogram parameters as explanatory variables in regression analysis of miticide bioactivity, and a regression model was successfully validated with independent data.

Based on experimental manipulation of HI data, we increased overall stochastic variance by 2.5% or 5.0% and showed that nugget and sill values increased 5.0 and 10%, respectively, while range values were less affected (Figure 5). For comparison, we can select, for instance, 25 or 100 random numbers and calculate their variance. Multiply each number by 1.025 (to add 2.5%), and the new variance is about 2.5% higher—in other words, the variance increases proportionally with the random numbers. However, sill and nugget values doubled in response to value increases. This simple phenomenon may explain why subtle changes in reflectance values do not show statistical difference in common parametric statistical analyses but indeed contribute significantly when HI data are analyzed in the context of a spatial data structure analysis. Our experimental manipulation of spectral data also showed that there was little difference between increasing all reflectance values by 2.5% or increasing a random selection of half of the reflectance values by 2.5%. Randomly increasing a random half (or any other portion) of the reflectance values may be considered a simplified simulation of a fairly uniform spray application (assuming that the liquid sprayed is brighter than the surface), and it generated a clearly detectable change in sill and nugget values.

References

1. Kim, M.S.; Chen, Y.R.; Mehl, P.M. Hyperspectral reflectance and fluorescence imaging system and safety. *Trans ASAE* **2001**, *44*, 721-729.
2. Mehl, P.M.; Chen, Y.; Kim, M.S.; Chan, D.E. Development of hyperspectral imaging technique for the detection of apple surface defects and contaminations. *J. Food Eng*. **2004**, *61*, 67-81.
3. Vargas, A.M.; Kim, M.S.; Tao, Y.; Lefcourt, A.M.; Chen, Y.-R.; Luo, Y.; Song, Y.; Buchanan, R. Detection of fecal contamination on cantaloupes using hyperspectral fluorescence imagery. *J. Food Sci.* **2005**, *70*, 471-476.
4. Lefcout, A.M.; Kim, M.S. Technique for normalizing intensity histograms of images when the approximate size of the target is known: Detection of feces on apples using fluorescence imaging. *Comput. Electron. Agric.* **2006**, *50*, 135-147.
5. Park, B.; Lawrence, K.C.; Windham, R.W.; Smith, D.P. Performance of hyperspectral imaging system for poultry surface fecal contaminant detection. *J. Food Eng.* **2006**, *75*, 340-348.
6. Haché, C.; Shibusawa, S.; Sasao, A.; Suhama, T.; Sah, B.P. Field-derived spectral characteristics to classify conventional and conservation agricultural practices. *Comput. Electron. Agric.* **2007**, *57*, 47-61.
7. Miao, G-X.; Müller, M.; Moodera, J.S. Magnetoresistance in double spin filter tunnel junctions with nonmagnetic electrodes and its unconventional bias dependence. *Phys. Rev. Lett.* **2009**, *102*, doi:10.1103/PhysRevLett.102.076601.
8. Pierna, J.A.F.; Baeten, V.; Renier, A.M.; Cogdill, R.A.; Dardenne, P. Combination of support vector machines (SVM) and near infrared (NIR) imaging spectroscopy for the detection of meat and bonemeal (MBM) in compound feeds. *Chemometrics.* **2004**, *18*, 341-349.
9. Gowen, A.A.; O'Donnell, C.P.; Taghizadeh, M.; Gaston, E., O'Gorman, A.; Cullen, P.J.; Frias, J.M.; Esquerre; C.; Downey, G. Hyperspectral imaging for the investigation of quality deterioration in sliced mushrooms (*Agaricus bisporus*) during storage. *Sens. Instrum. Food Qual. Safety* **2007**, *2*, 133-143.

10. Garcia-Allende, P.B.; Conde, O.M.; Mirapeix, J.; Cobo, A.; Lopez-Higuera, J.M. Quality control of industrial processes by combining a hyperspectral sensor and Fisher's linear discriminant analysis. *Sensor. Actuator. B-Chem.* **2008**, *129*, 977-984.

11. Nansen, C.; Kolomiets, M.; Gao, X. Considerations regarding use of hyperspectral imaging data in classifications of food products—exemplified by analysis of maize kernels. *J. Agr. Food Chem.* **2008**, *56*, 2933-2938.

12. Kolomiets, O.; Hoffmann, U.; Geladi, P.; Siesler, H.W. Quantitative determination of pharmaceutical drug formulations by near-infrared sprotroscopic imaging. *Appl. Spectrosc.* **2008**, *62*, 1200-1208.

13. Hunt, G.R. Spectroscopic properties of rocks and minerals. In *Handbook of Physical Properties of Rocks*, Carmichael, R.S., Ed.; CRC Press: Boca Raton, FL, USA, 1982; pp. 295-385.

14. Abidi, N.; Hequet, E. Fourier Transform Infrared analysis of cotton contamination. *Textile Res. J.* **2007**, *77*, 77-84.

15. Abidi, N.; Hequet, E.. Fourier Transform Infrared analysis of trehalulose and sticky cotton yarn defects using ZnSe-Diamond Universal Attenuated Total Reflectance. *Textile Res. J.* **2005**, *75*, 645-652.

16. Abidi, N.; Hequet, E.; Cabrales, L.; Gannaway, J.; Wilkins, T.; Wells, L.W. Evaluating cell wall structure and composition of developing cotton fibers using Fourier transform infrared spectroscopy and thermogravimetric analysis. *J. Appl. Polym. Sci.* **2008**, *107*,476-486.

17. McCann, M.C.; Defernez, M.; Urbanowicz, B.R.; Tewari, J.C.; Langewisch, T.; Olek, A.; Wells, B.; Wilson, R.H.; Carpita, N.C. Neural network analyses of infrared spectra for classifying cell wall architectures. *Plant Physiol.* **2007**, 143, 1314-1326.

18. Yong, W.; Link, B.; O'Malley, R.; Tewari, J.; Hunter, C.T.; Lu, C.-A.; Li, X.; Bleecker, A.B.; Koch, K.E.; McCann, M.C.; McCarty, D.R.; Patterson, S.E.; Reiter, W.-D.; Staiger, C.; Thomas, S.R.; Vermerris, W.; Carpita, N.C. Genomics of plant cell wall biogenesis. *Planta* **2005**, *221*, 747-751.

19. Carpita, N.C.; Defernez, M.; Findlay, K.; Wells, B.; Shoue, D.A.; Catchpole, G.; Wilson, R.H.; McCann, M.C. Cell wall architecture of the elongating Maize Coleoptile. *Plant Physiol.* **2001**, *127*, 551-565.

20. Zeier, J.; Schreiber, L. Fourier transform infrared-spectroscopic characterization of isolated endodermal cell walls from plant roots: chemical nature in relation to anatomical development. *Planta.* **1999**, *209*, 537-542.

21. Chen, L.; Carpita, N.C.; Reiter, W.-D.; Wilson, R.H.; Jeffries, C.; McCann, M.C. A rapid method to screen for cell-wall mutants using discriminant analysis of Fourier transform spectra. *Plant J.* **1998**, *16*, 385-392.

22. McCann, M.C.; Chen, L.; Roberts, L.; Kemsley, E.K.; Sene, C.; Carpita, N.C.; Stacey, N.J.; Wilson, R.H. Infrared microspectroscopy: sampling heterogeneity in plant cell wall composition and architecture. *Physiol Plant.* **1997**, *100*, 729-738.

23. Séné, C.F.B.; McCann, M.C.; Wilson, R.H.; Grinter, R. Fourier-transform Raman and Fourier-transform infrared spectroscopy an investigation of five higher plant cell walls and their components. *Plant Physiol.* **1994**, *106*, 1623-1631.

24. McCann, M.C.; Stacey, N.J.; Wilson, R.; Roberts, K. Orientation of macromolecules in the walls of elongating carrot cells. *J. Cell Sci.* **1993**, *106*, 1347-1356.

25. McCann, M.C.; Wells, B.; Roberts, K.; Complexity in the spatial localization and length distribution of plant cell-wall matrix polysaccharides. *J. Microsc*. **1992**, *166*, 123-136.

26. Rutlidge, H.T.; Reedy, B.J. Classification of heterogeneous solids using infrared hyperspectral imaging. *Appl. Spectrosc.* **2008**, *63*, 162-179.

27. Kong, S.G.; Chen, Y.; Kim, I.; Kim, M.S. Analysis of hyperspectral fluorescence images for poultry skin tumor inspection. *Appl. Optics*. **2004**, *43*, 824-832.

28. Qiao, J.; Ngadi, M.O.; Wang, N.; Garieepy, C.; Prasher, S.O. Pork quality and marbling level assessment uing a hyperspectral imaging system. *J. Food Eng.* **2007**, *83*, 10-16.

29. Delwiche. S.R. Protein content of single kernels of wheat by near-infrared reflectance spectroscopy. *J. Cereal Sci.* **1996**, *27*, 241-254.

30. Cogdill, R.; Hurburgh, C.; Rippke, G. Single-kernel maize analysis by near-infrared hyperspectral imaging. *Trans. ASAE* **2004**, *47*, 311-320.

31. Zhao, D.K.; Raja Reddy, K.;. Kakani, V.G.; Read, J.J.; Carter, G.A. Corn (*Zea mays* L) growth, leaf pigment concentration, photosynthesis and leaf hyperspectral reflectance properties as affected by nitrogen supply. *Plant Soil* **2003**, *257*, 205-217.

32. El-Sebai, O.A.; Sanderson, R.; Bleiweiss, M.P.; Schmidt, N. Detection of Sitotroga cerealella (Olivier) infestation of wheat kernbels using hyperspectral reflectance. *J. Entomol. Sci.* **2006**, *41*, 155-164.

33. Campbell, P.K.E.; Middleton, E.M.; McMurtrey, J.E.; Corp, L.A.; Chappelle, E.W. Assessment of vegetation stress using reflectance or fluorescence measurements. *J. Environ. Qual.* **2007**, *36*, 832-845.

34. Goel, P.K.; Prasher, S.O.; Patel, R.M.; Landry, J.A.; Bonnell, R.B.; Viau, A.A. Classification of hyperspectral data by decision trees and artificial neural networks to identify weed stress and nitrogen status of corn. *Comput. Electron. Agric.* **2003**, *39*, 67-93.

35. Jiang, L.; Zhu, B.; Rao, X.; Berney, G.; Tao, Y. Discrimination of black walnut shell and pulp in hyperspectral fluorescence imagery using Gaussian kernel function approach. *J. Food Eng.* **2007**, *81*, 108-117.

36. Isaaks, E.H.; Srivastava, R.M. *Applied Geostatistics*; Oxford University Press: New York, NY, USA, 1989.

37. Liebhold, A.M.; Rossi, R.E.; Kemp, W.P. Geostatistics and geographic information systems in applied insect ecology. *Ann. Rev. Entomol*. **1993**, *38*, 303-327.

38. Brenner, R.J.; Focks, D.A.; Arbogast, R.T.; Weaver, D.K.; Shuman, D. Practical use of spatial analysis in precision targeting for integrated pest management. *Am. Entomol*. **1998**, *44*, 79-101.

39. Liebhold, A.M.; Sharov, A.A. Testing for correlation in the presence of spatial autocorrelation in insect count data. In *Population and Community Ecology for Insect Management and Conservation*; Baumgartner, J., Brandmayr, P., Manly, B.F.J., Eds.; A. A. Balkema: Rotterdam, the Netherlands, 1998; pp. 111-117.

40. Rossi, R.E.; Mulla, D.J.; Journel, A.G.; Franz, E.H. Geostatistical tools for modeling and interpreting ecological spatial dependence. *Ecol. Monogr*. **1992**, *62*, 277-314.

41. Nansen, C.; Hinson, B.; Davidson, D.; Vaughn, K.; Hosseini, A. Novel approaches to application and performance assessment of insecticide applications to crop leaves. *J. Econ. Entomol.* **2009**, Accepted.

42. Porter, P.; Troxclair, N.; Schuster, G., Porter, D.O.; Cronholm, G.; Bynum, E., Jr.; Patrick, C.; Davis, S.G. *Texas Corn Production: Emphasizing Pest Management & Irrigation*; Texas Cooperative Extension, The Texas A&M University System: College Station, TX, USA, 2005; B-6177, 08/05.

43. Smith, B. *Infrared Spectral Interpretation: A Systematic Approach*; CRC Press: New York, NY, USA, 1999.

44. Gopal, M.; Mishra E. Analytical method for estimation of a new insecticide Flubendiamide and its safety evaluation for usage in rice crop. *Bull. Environ. Contam. Toxicol.* **2008**, *81*, 360-364.

45. Sharma, A.; Gupta, M.; Shanker, A. Fenvalerate residue level and dissipation in tea and in its infusion. *Food Add. Contam.* **2008**, *25*, 97-104.

46. Zhang, Q.; Sun, Q.; Hua, B.; Shen, Q.; Yang, G.; Liang, X.; Sun, X.;, Liu, F. Development of a sensitive ELISA for the analysis of the organophosphorous insecticide fenthion in fruit samples. *Food Chem.* **2008**, *106*, 1278-1284.

47. Arrebola, F.J.; Martínez Vidal, J.L.; González-Rodríguez, M.J.; Garrido-Frenich, A.; Sánchez Morito, N. Reduction of analysis time in gas chromatography. Application of low-pressure gas chromatography-tandem mass spectrometry to the determination of pesticide residues in vegetables. *J. Chrom. A.* **2003**, *1005*, 131-141.

48. Caldas, E.; Jardim, A.; Ambrus, A.; Souza, L.C. Variability of organophosphorus insecticide residues in large size crops grown in commercial farms in Brazil. *Food Add. Contam.* **2006**, *23*, 148-158.

49. Baghzouz, M.; Devitt, D.A.; Morris, R.L. Evaluating temporal variability in the spectral reflectance response of annual ryegrass to changes in nitrogen applications and leaching fractions. *Int. J. Remote Sens.* **2006**, *27*, 4137-4157.

50. Okamoto, H.; Lee, W.S. Green citrus detection using hyperspectral imaging. *Comput. Electron. Agric.* **2009**, *66*, 201-208.

51. Nansen, C.; Macedo, T.; Swanson, R.; Weaver, D.K. Use of spatial structure analysis of hyperspectral data cubes for detection of insect-induced stress in wheat plants. *Int. J. Remote Sens.* **2009**, *30*, 2447-2464.